JOURNAL OF MATERIALS SCIENCE 35 (2000) 5691 – 5698

Hardfacing of stainless steel with laser melted colmonoy

T. A. M. HAEMERS, D. G. RICKERBY, F. LANZA, F. GEIGER
Institute for Advanced Materials, Commission of the European Communities, Joint Research Centre, 21020 Ispra, Varese, Italy

E. J. MITTEMEIJER
Max Planck Institute for Metals Research, Seestrasse 92, 71074 Stuttgart, Germany; Laboratory of Materials Science, Delft University of Technology, Rotterdamseweg 137, 2628 AL Delft, The Netherlands
E-mail: mittemeijer@mf.mpi-stuttgart.mpg.de

Stainless steel substrates were hardfaced with laser melted Colmonoy applying a continuous wire injection technique using a CO_2 laser. The microstructures of single pass laser clad deposits were examined and related to workpiece traverse velocity at constant laser output. Particular attention was paid to the effect of dilution of the cladding alloy due to convectional mixing with the partially melted substrate material. The solidification microstructure of the rapidly cooled cladded layer consisted predominantly of nickel rich cellular dendrites and interdendritic lamellar eutectic borides.

1. Introduction

Applying a coating of a hardfacing alloy to the surface of a stainless steel component can be an effective means for wear reduction. One technique to produce such a coating involves cladding of the coating material by the use of a high power laser as the heat source. During the cladding process part of the substrate melts, and mixes with the coating due to the convection in the melt pool. In this way the composition of the layer becomes different from the nominal composition of the used coating alloy, which changes the properties of the coating with respect to those of the alloy used for coating formation.

As compared to manual welding methods [1] the above noted mixing of coating materials and substrate material is less severe using a laser because of its more localised heat input. Further, to obtain a relatively thick surface layer, multiple laser passes are needed, and thus the composition at the outer surface of the total layer can be closer to that of the alloy used for coating formation.

The Ni-Cr-B-Si hardfacing alloy Colmonoy was used here to coat stainless steel substrates by applying the continuous wire injection technique using a CO_2 laser. Colmonoy can have high hardness, wear resistance and corrosion resistance [2]. One advantage of using the continuous wire injection technique is that this procedure uses the same type of wire as used in MIG (metal-inert gas) welding. With respect to the remelting of predeposited layers, the advantage of using this technique is that it is in essence a single step process, and that the thickness of the layer is less critical with respect to the resulting microstructure than for remelted plasma spray deposits [3].

In the solidification of alloy welds the constitutional undercooling [4–6] has an important influence on the resulting microstructure. Constitutional undercooling depends on the partition coefficients of the elements, the temperature gradients, and the solidification velocity. A cellular or a dendritic structure can occur with metallic (Ni, Fe) dendrites. Since the solubility of boron in nickel is low (0.003 at%) [7], the boron is expected to segregate completely into the interdendritic region. This region will then solidify as a boride/metal eutectic. According to Ref. 8 the coating properties are dominated by the Ni_3B/Ni rich eutectic, and the hardness of the resulting structure can correlate with the secondary dendrite spacing.

2. Experimental

Using a Colmonoy 5 wire (for composition, see Table I) cladding occurred by applying a Rofin Sinar CO_2 laser at a continuous power output of 3.9 kW. The coatings were made by depositing adjacent traces (spacing 2.0 mm) of Colmonoy 5 on a substrate of AISI 316L stainless steel (for composition, see Table I). The welding wire of 1.7 mm diameter was fed to the substrate, on a table, using a Kematig wire feed at the same velocity as the table velocity. Argon was used as protective gas with a flow of 15 l/min. A spot diameter of 2.0 mm, larger than the wire thickness, was used, giving a power density in the order of 10^5 W/cm^2. Single pass coatings with a thickness between 1 and 2 mm were made with three workpiece traverse velocities of 0.5 cm/s, 1.1 cm/s and 2.0 cm/s, and a three-layer deposit was produced with a thickness between 2.5 and 3 mm, employing a workpiece velocity of 1.1 cm/s (see Fig. 1).

X-ray diffraction data were taken with copper Kα radiation, using a PHILIPS PW1830 diffractometer, with a Ni filter, from unpolished specimens (i.e. as obtained after the laser treatment) and from specimens that

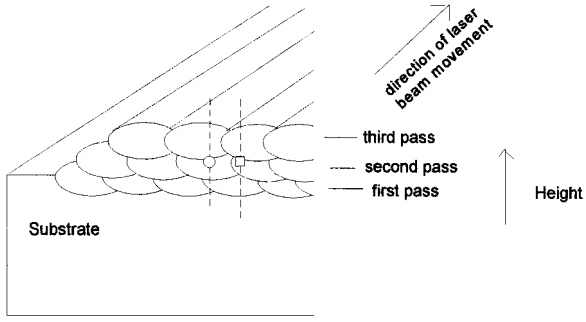

Figure 1 Schematic picture of three layer deposit. The ellipses represent single traces. The first layer is deposited by depositing slightly overlapping traces next to each other. The traces of the subsequent layers are deposited in the troughs of the underlying pass. The dashed vertical lines pertain to the hardness-depth profiles shown in Fig. 11.

TABLE I Composition of used alloys

		Ni	Fe	Cr	B	Mo	Si	Mn	C
Colmonoy 5	wt%	77.5	3.0	11.5	2.5		3.8	1.0	0.7
(coating)	at%	64.8	2.6	10.9	11.3		6.6	0.9	2.9
AISI 316L	wt%	11.0	67.9	17.0		2.2	0.35	1.5	0.02
(substrate)	at%	10.4	67.8	18.2		1.3	0.7	1.5	0.1

were electrochemically polished using a 50% H_3PO_4, 30% H_2SO_4, 20% H_2O solution at 5 V after removing 0.2 mm of the surface layer by mechanically polishing.

Cross sectional specimens for examination by optical microscopy and SEM were etched with 50% HNO_3 (Nital). Hardness was measured using a Leitz Miniload 2 hardness tester applying a load of 50 g.

Planar sections for TEM observation were prepared by cutting from the cladded layer, mechanically thinning, and jet polishing using a $HClO_4$, acetic acid solution (Struers electrolyte A8-I) at 65 V. The resulting foils were examined with a JEOL 200CX transmission

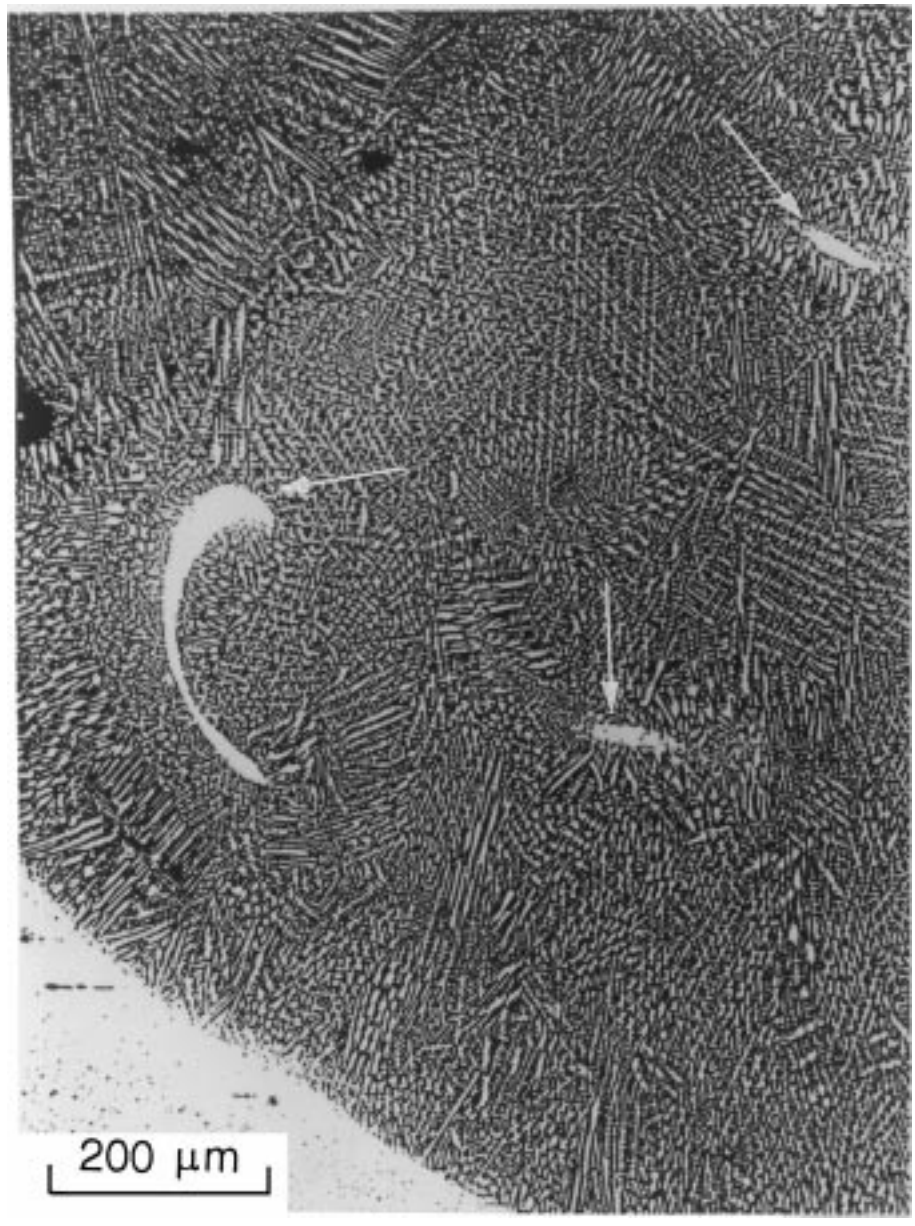

Figure 2 Optical micrograph of a cross section of the three layer coating (table velocity 1.1 cm/s) at the interface with the substrate.

electron microscope operating at 200 kV. Qualitative composition data were taken from the TEM specimens with a Kevex Energy Dispersive Spectrometry (EDS) system using the STEM unit attachment of the JEOL 200CX transmission electron microscope. SEM observations were made with the STEM attachment unit of the TEM.

3. Results and Discussion

3.1. Morphology and crystallography

3.1.1. Optical, scanning and transmission electron microscopy

The optical micrographs show a dendritic structure (see the fine light structure visible in Figs 2 and 3). The orientations of the dendrites are related to the local solidification direction in the melt [5]. At the interface with the substrate the dendrites are oriented on average perpendicular to the interface (Fig. 2). In the top left part of Fig. 2 the interface of the first pass and the second pass is visible. At this interface the dendrites start to grow with an orientation perpendicular to the interface in the same way as at the interface of the first pass with the substrate. On the top of the three-layer specimen the main orientation of the dendrites is perpendicular to the cross section (i.e. perpendicular to the plane of Fig. 3) and corresponds to the welding direction (i.e. the direction of the laser beam relative to the specimen).

Another feature that can be observed in Fig. 2 is the presence of substrate material in the coating (see arrows in Fig. 2). This substrate material may have been loosened from the substrate by the strong convection currents in the melt [9, 10].

The structure in the interdendritic regions cannot be revealed by optical microscopy. SEM and TEM observations were made of planar sections taken from the 0.5 cm/s and the 1.1 cm/s single pass coating specimens (see Figs 4–6). First note that in the SEM micrograph the dendrites appear dark (Fig. 4), whereas in the TEM micrographs (Fig. 5) the dendrites appear bright. Then it follows from Figs 4 and 5 that the interdendritic regions exist of a fine scale eutectic structure (lamellar spacing of the order of 0.1 μm). Further, branching

Figure 3 Optical micrograph of a cross section of the three layer coating (table velocity 1.1 cm/s) at the top of the coating.

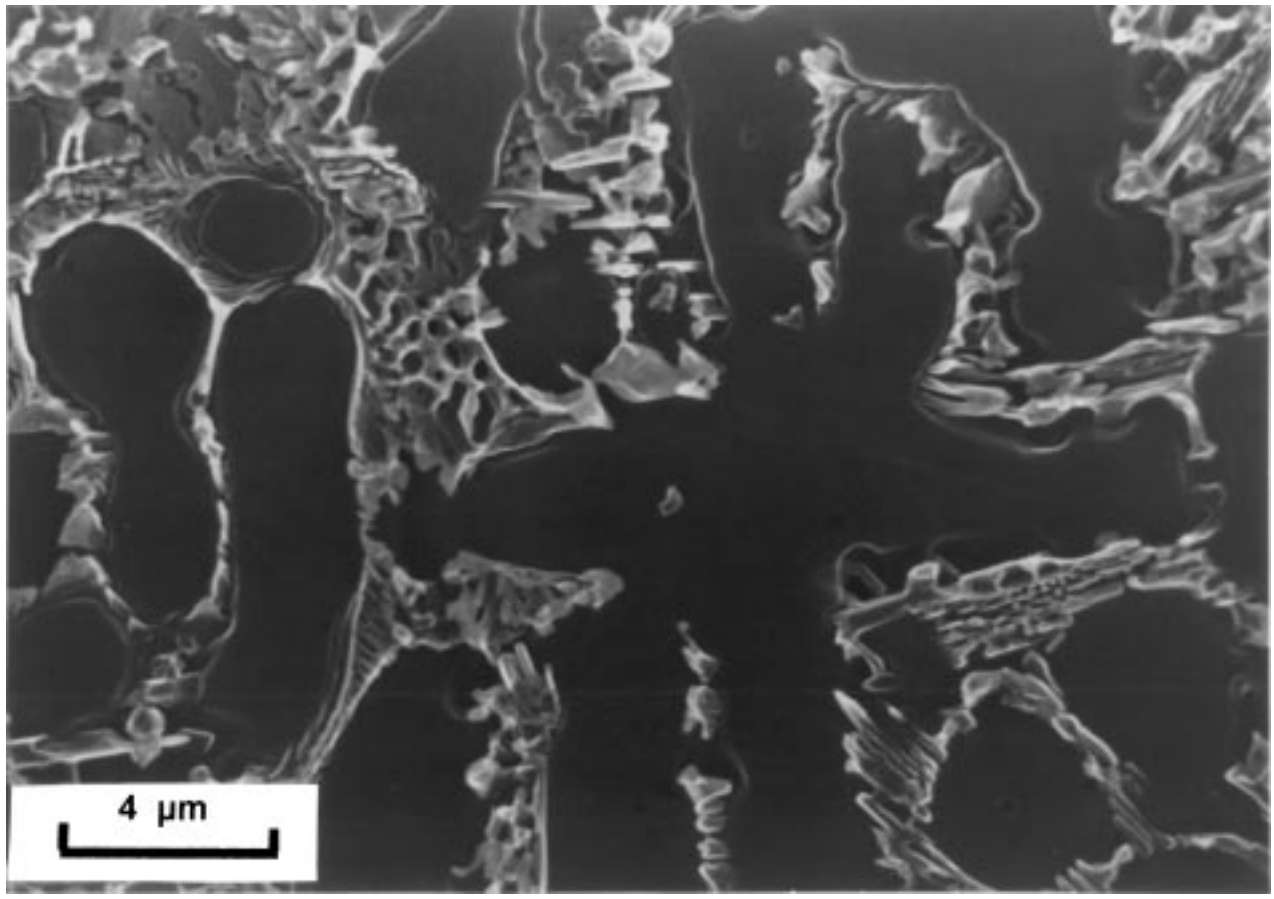

Figure 4 Scanning electron micrograph of single layer coating applied with a table velocity of 1.1 cm/s. The micrograph shows several dendrites and an eutectic structure in the interdendritic regions. Further, note the branching of the dendrites at right angles.

Figure 5 TEM micrograph of single layer Colmonoy coating applied with a table velocity of 1.1 cm/s. The micrograph shows a secondary dendrite arm with dislocations in the metal matrix. Further, the eutectic structure of the interdendritic part is recognisable and has a lamellar spacing of the order of 0.1 μm.

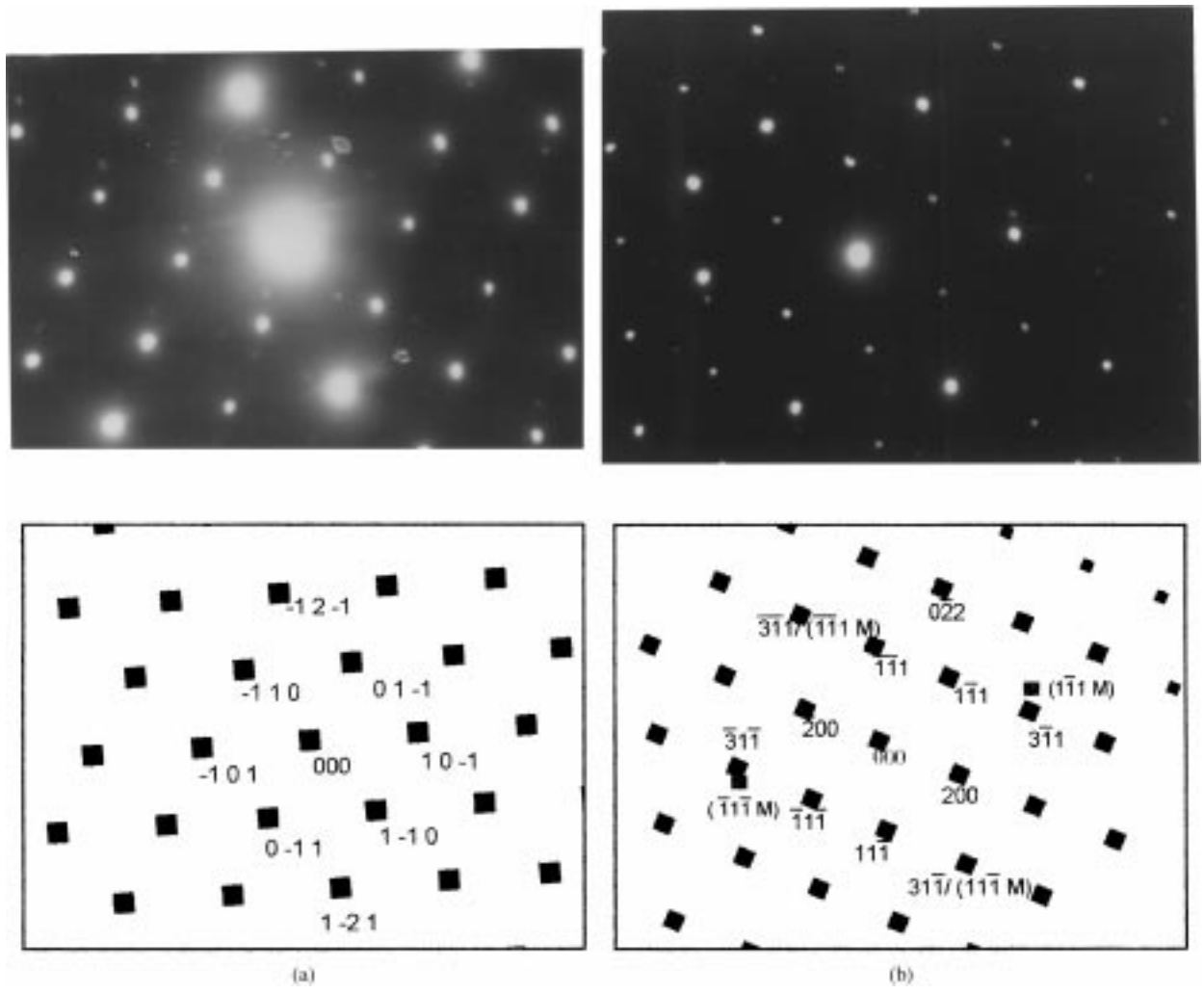

Figure 6 (a) Selected area diffraction pattern of phase in the interdendritic eutectic, indexed as a [111] zone axis pattern of a cementite-like orthorhombic phase, probably (Ni, Fe)$_3$ (B, C); (b) Selected area diffraction pattern of phase in the interdendritic eutectic, indexed as a [011] zone axis pattern of a Mn_4B-like pseudo hexagonal orthorhombic phase, probably Cr_2B. The spots indicated with M are from the f.c.c. metal matrix.

of the dendrite arms in perpendicular directions is observed in Fig. 4, and dislocations can be observed in the dendrites (Fig. 5).

Selected area diffraction patterns from the dendritic regions exhibit a face centred cubic crystal structure, as expected for a NiFe solid solution.

Applying selected area diffraction to the eutectic interdendritic regions, two different boride phases could be identified (Fig. 6; see also Table II): The diffraction pattern of Fig. 6a was interpreted as the [1 1 1] zone axis pattern of a cementite-like structure (space group Pnma), which for the present system could correspond with a (Ni, Fe)$_3$ (B, C) solid solution. The diffraction pattern of Fig. 6b was interpreted as the [0 1 1] zone axis pattern of a Mn_4B type (space group Fddd) pseudo-hexagonal orthorhombic structure. The only known such boride phase that appears compatible with the composition of the present alloy is Cr_2B [2]. According to the isothermal section of the ternary Ni-Cr-B phase diagram at 1000 K the only chromium boride that can coexist with Ni_3B in equilibrium is CrB [2]. It is be suggested that a similar conclusion would hold for the present case, i.e. the (Ni, Fe)$_3$ (B, C) phase plays the role of Ni_3B. Then the occurrence of a Cr_2B phase should be interpreted as a non-equilibrium feature. In laser melting the solidification velocity can be fast enough to give rise to phases that are metastable in view of prevailing pressure, temperature and composition of the alloy.

TABLE II Unit cell parameters used for indexing diffraction patterns

(Ni, Fe)$_3$ (B, C)	$a = 0.1527$ nm,	$b = 0.66$ nm,	$c = 0.44$ nm; present X-ray data
Cr_2B	$a = 0.74$ nm,	$b = 0.47$ nm,	$c = 0.425$ nm; data from ref. 13.

A high magnification picture (bright field) taken from the interdendritic region suggests the occurrence of planar defects (Fig. 7). The diffraction pattern of this area can indeed be interpreted as a superposition of two twin related patterns of (Ni, Fe)$_3$ (B, C), both with [1 0 0] zone axis, and a [0 0 1] zone axis pattern of Cr_2B (see Fig. 8). Therefore the planar defects in Fig. 7 can be interpreted as a stacking of twinned (Ni, Fe)$_3$ ((B, C) layers with the (0 1 1) plane of (Ni, Fe)$_3$ (B, C) as twinning plane and Cr_2B layers with the (0 1 0) plane of Cr_2B parallel to the twinning plane of (Ni, Fe)$_3$ (B, C). The diffraction spots that coincide in the pattern are the (0 1 1) spots of (Ni, Fe)$_3$ (B, C) and the (0 4 0)

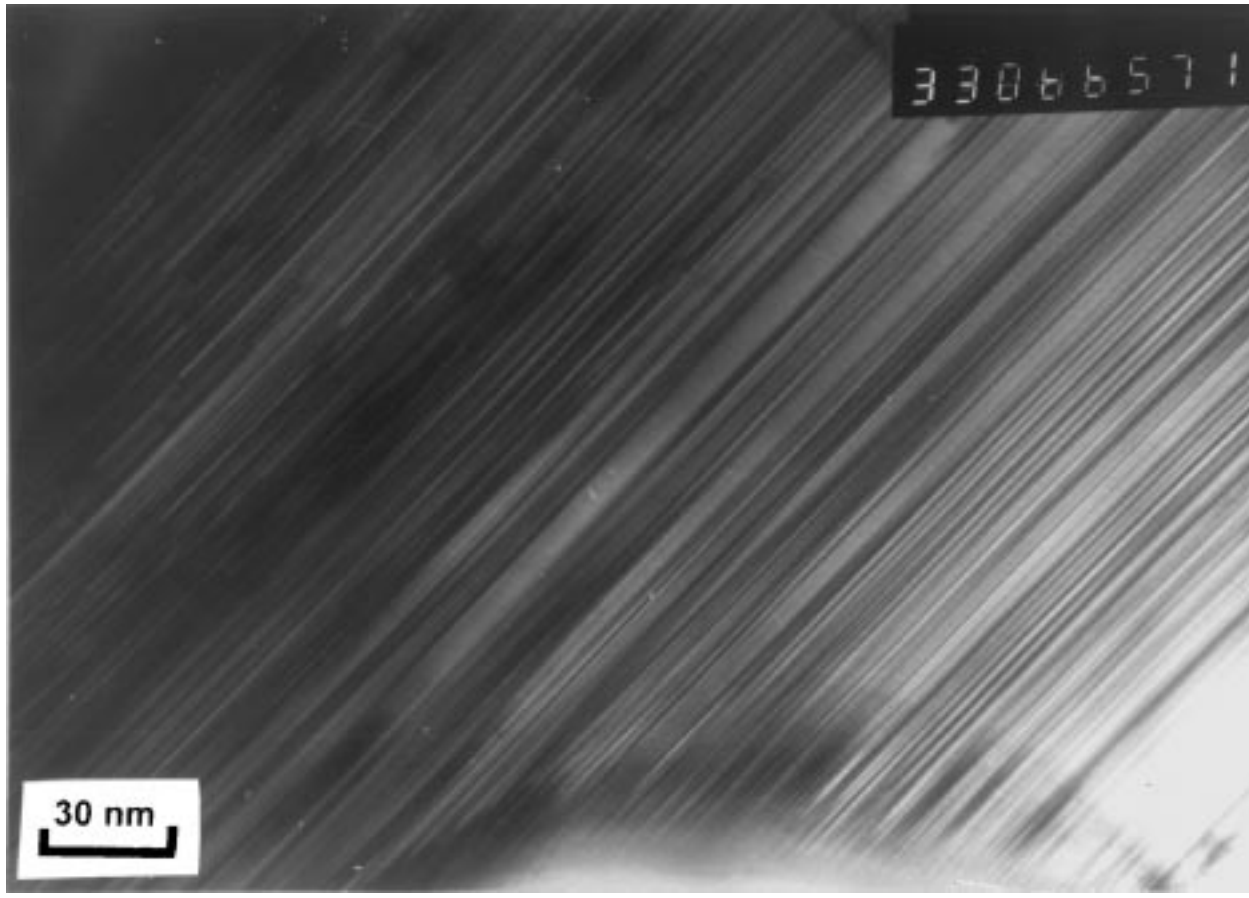

Figure 7 Bright field transmission electron micrograph of interdendritic region. Note the banded structure suggesting the presence of planar defects. For interpretation, see text and Fig. 8.

spot of Cr_2B. This suggest the following orientation relationships:

a) $(0\ 1\ 1)_{(Ni,Fe)_3(B,C)}//(0\ 1\ 0)_{Cr_2B}$;

$[1\ 0\ 0]_{(Ni,Fe)_3(B,C)}//[1\ 0\ 0]_{Cr_2B}$

b) $(0\ 1\ 1)_{(Ni,Fe)_3(B,C)(twin)}//(0\ -1\ 0)_{Cr_2B}$;

$[-1\ 0\ 0]_{(Ni,Fe)_3(B,C)twin)}//[1\ 0\ 0]_{Cr_2B}$

3.1.2. X-ray diffraction

The X-ray diffraction patterns of the 0.5 cm/s and 1.1 cm/s specimens show only evidence of a f.c.c. phase. This phase has a lattice parameter of $a = 0.356$ nm suggesting a Ni rich metallic phase. Only for the 2.0 cm/s specimen (Fig. 9) and the three-layer specimens diffraction lines from a second phase can be discerned. These lines can be indexed according to an orthorhombic cementite (Pnma)-like structure, as also observed by TEM (see above), and that could correspond with a $(Ni, Fe)_3$ (B, C) solid solution. The values obtained for its lattice parameters are: $a = 0.526$ nm, $b = 0.661$ nm, $c = 0.441$ nm. If this phase would be pure Ni_3B the expected values for the unit cell parameters are: $a = 0.5211$ nm, $b = 0.6619$ nm, $c = 0.4389$ nm [11]. The differences between these values for the lattice parameters and the observed ones could be due to the presence of Fe on Ni sites, recognising that Fe has a larger atomic size then Ni.

3.2. Compositional variation

EDS analysis carried out in the electron microscope (cf. Section 2) indicates small differences in composition between specimens of different table velocities. The ratio of the Fe K_α and Ni K_α peaks is larger for the 0.5 cm/s specimen than for the 1.1 cm/s specimen. Recognising that the surface region of the steel substrate melts upon passage of the laser beam, this could be interpreted as that more iron from the substrate is incorporated into the coating at lower table velocities, as could be due to a larger incorporation of melted substrate material into the coating at lower table velocities: at lower table velocities both the energy density and the interaction time are larger, implying that a thicker layer of the substrate melts and that the weld stays liquid for a longer time enhancing mixing of substrate and coating.

The compositional variation across a dendrite and into the interdendritic region was analysed in the electron microscope using EDS. Composition data were determined at intervals of 300 nm applying a Cliff-Lorimer analysis using the calibration factors as determined in a previous study using the same instrument at 200 kV [12]. Results are shown in Fig. 10. Proceeding from the centre to the edge of the dendrite, upon traversing the interface with the interdendritic region a sharp increase in Cr content and a sharp decrease in Ni content are observed, whereas no such abrupt change is observed for the Fe content. Clearly, the dendrites are Ni rich and Cr poor, and visa versa for the eutectic interdendritic regions. Furthermore, the relatively high

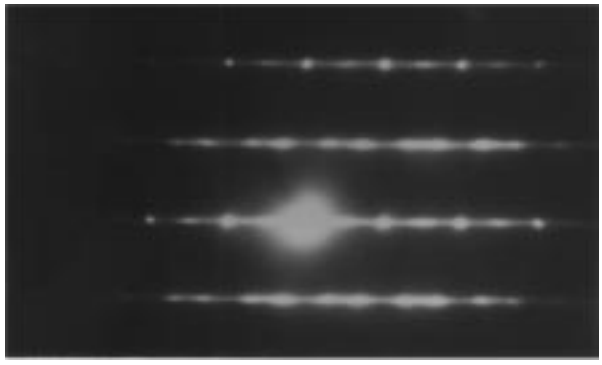

(a)

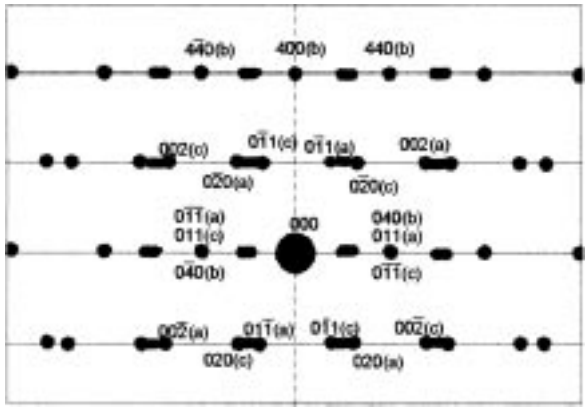

(b)

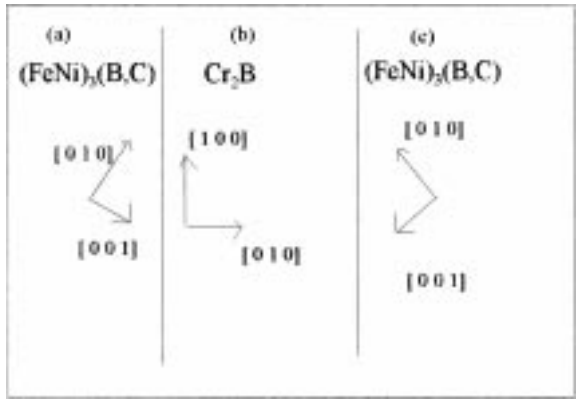

(c)

Figure 8 (a) Selected area diffraction pattern of region shown in Fig. 7; (b) Interpretation and indexing of selected area diffraction pattern shown in Fig. 8a. Superposition of twin related $(Ni, Fe)_3$ (B, C) diffraction patterns with [1 0 0] zone axis and a single [0 0 1] zone axis pattern of Cr_2B. The dashed vertical line indicates the twinning/mirror plane in the diffraction pattern. The lines correspond with the lines in the diffraction pattern. For meaning of (a), (b) end (c), see Fig. 8c; (c) Schematic interpretation of the stacking in the banded structure of Fig. 7. The twinning of $(Ni, Fe)_3$ (B, C) is assumed to be caused by the structural relationship between its (0 1 1) twin planes and the (0 1 0) plane of Cr_2B.

Cr content in the eutectic interdendritic region is consistent with the possible presence of Cr_2B instead of CrB; see result and discussion in Section 3.1.

3.3. Hardness-depth profiles

The hardness was measured in cross-sections along lines as indicated in Fig. 1 (results in Fig. 11). The hardness has a value of approximately 500 Hv on the surface and in the upper 2 mm of the coated layer. As follows from the hardness profile indicated with symbol

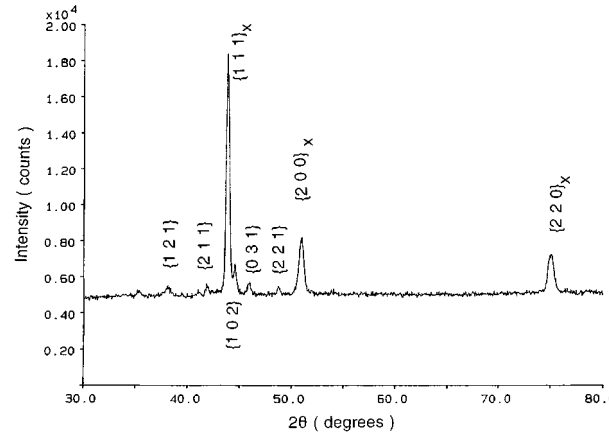

Figure 9 X-ray diffraction pattern of the 2.0 cm/s specimen. Copper K_α radiation. Lines marked with x are from the f.c.c. phase.

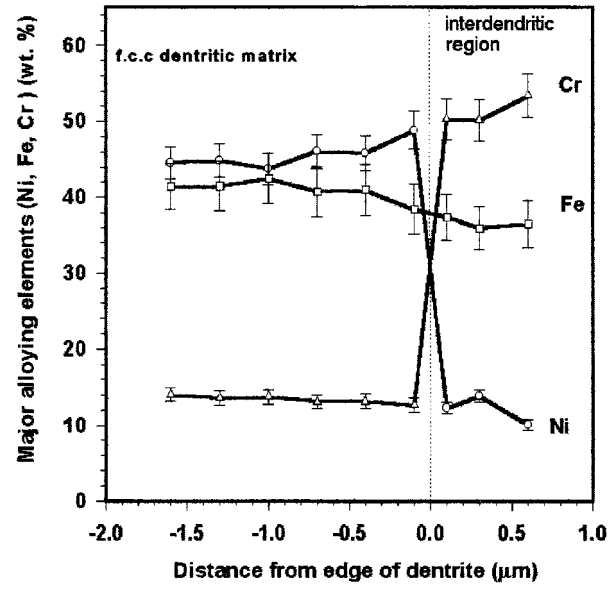

Figure 10 EDS trace across dendrite/eutectic interdendritic interface. For this figure the sum of the amounts of Cr, Fe and Ni has been set equal to 100%, thus ignoring the minor presence of other elements.

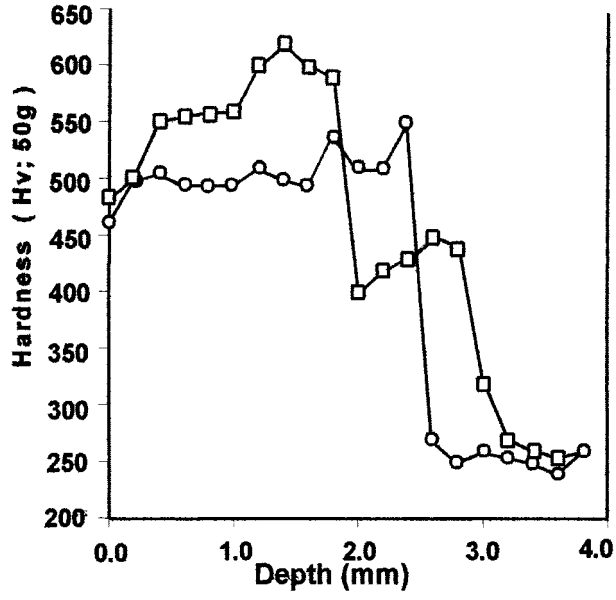

Figure 11 Hardness profiles of the three-layered specimen, workpiece velocity 1.1 cm/s, measured in cross-section from the surface into the layers. The symbols "□" and "○" refer to the lines indicated in Fig. 1.

"□" the hardness of the core of a trace of the first pass is lower: see drop from significantly more then 500 Hv to about 400 Hv in Fig. 11 Above the edges of the traces of the first pass no such drop in hardness is measured (see data indicated with symbol "○"). Obviously, upon crossing the layer-substrate interface the hardness drops abruptly.

One might suggest that the lower value of the hardness in the core of the trace of the first pass is related to both a relatively large dendrite size and a relatively large dilution with substrate material. However, the difference in dendrite size between sublayers deposited in consecutive passes (see Fig. 2) is too small to account for the difference in hardness if the hardness of this type of alloy coatings is related to the secondary dendrite arm spacing [8]. Therefore, it is more probable that the lower hardness for the material applied by the first pass can be ascribed to a relatively large mixing with substrate material that would result in a relatively small amount of the hard boride phases, as compared to the material applied in the traces of the second and third passes.

4. Conclusions

1. The solidification microstructure of the Colmonoy alloy applied by laser beam melting to a stainless steel substrate is dendritic with a eutectic interdendritic region.

2. On the basis of X-ray diffraction and selected area electron diffraction analyses and composition analysis it followed that the dendritic, matrix phase is of f.c.c. type and is likely a (Ni, Fe) solid solution, and the eutectic, interdendritic region is composed of two boride phases: a cementite-like one $(Ni, Fe)_3$ (B, C) solid solution and a pseudo-hexagonal, orthorhombic one Cr_2B.

3. In the boride phases a high density of planar defects is found. The defects are interpreted as a stacking of $(Ni, Fe)_3$ (B, C) and Cr_2B layers with orientational relationships, implying that two $(Ni, Fe)_3$ (B, C) layers, with one Cr_2B layer in between, are twin oriented:

$$(0\,1\,1)_{(Ni,Fe)_3(B,C)}//(0\,1\,0)_{Cr_2B};$$
$$[1\,0\,0]_{(Ni,Fe)_3(B,C)}//[1\,0\,0]_{Cr_2B}$$
$$(0\,1\,1)_{(Ni,Fe)_3(B,C)(twin)}//(0\,-1\,0)_{Cr_2B};$$
$$[-1\,0\,0]_{(Ni,Fe)_3(B,C)twin)}//[1\,0\,0]_{Cr_2B}$$

4. During the laser cladding process part of the substrate melts and mixes with the coating due to the convection in the melt pool. In this way the composition of the layer becomes different from the nominal composition of the coating alloy. At the location of most pronounced mixing with the substrate material, the lowest hardness is observed, which is ascribed to a relatively small amount of the boride phases.

Acknowledgements

The authors want to thank R. Zausch for the performing of the laser cladding and N. Wächter for the preparation of the TEM specimens.

References

1. R. M. MACINTYRE, in "Laser in Materials Processing," edited by E. A. Metzbower (American Society for Metals, U.S.A., 1983) p. 230.
2. O. KNOTEK, E. LUGSCHEIDER and H. REIMANN, *Journal of Vacuum Science and Technology* **12** (1975) 770.
3. B. L. MORDIKE and W. N. KAHRMANN, in "Laser Treatments of Materials," edited by B. L. Mordike (DGM informationsgesellschaft mbH, Oberursel, Germany, 1987) p. 383.
4. W. W. MULLINS and R. F. SEKERKA, *J. of Appl. Phys.* **35** (1964) 444.
5. S. A. DAVID and J. M. VITEK, *International Metals Rev.* **34** (1989) 213.
6. R. TRIVEDI and W. KURZ, *y Acta Metall. et Mater.* **42** (1994) 14.
7. O. TEPPO and P. TASKINEN, *Materials Science and Technology* **9** (1993) 205.
8. P. J. E. MONSON and W. M. STEEN, in "Laser Treatments of Materials," edited by. B. L. Mordike (DGM informationsgesellschaft mbH, Oberursel, Germany, 1987) p. 123.
9. H. J. HEGGE and J. TH. M. DE HOSSON, *J. of Materials Science* **26** (1991) 711.
10. S. KOU and Y. H. WANG, *Metallurgical Transactions A* **17A** (1986) 2265.
11. S. RUNDQVIST, *Acta Chem. Scand.* **13** (1959) 1193.
12. D. G. RICKERBY, in Emag '87, Workshop on Analytical Electron Microscopy, Manchester (IOP publishing, United Kingdom, 1987) p. 19.
13. F. BERTAUT and P. BLUM, *C.R. Acad. Sci. Paris* **236** (1953) 805.

Received 19 May 1999
and accepted 23 March 2000